

Free energy functionals for efficient phase field crystal modeling of structural phase transformations

Michael Greenwood,^{1,2} Nikolas Provatas,² and Jörg Rottler¹

¹*Department of Physics and Astronomy, University of British Columbia,
6224 Agricultural Road Vancouver, BC, V6T 1Z1, Canada*

²*Department of Materials Science and Engineering, McMaster University,
1280 Main Street West, Hamilton, Ontario, L8S 4L7, Canada*

The phase field crystal (PFC) method has emerged as a promising technique for modeling materials with atomistic resolution on mesoscopic time scales. The approach is numerically much more efficient than classical density functional theory (CDFT), but its single mode free energy functional only leads to lattices with triangular (2D) or BCC (3D) symmetries. By returning to a closer approximation of the CDFT free energy functional, we develop a systematic construction of two-particle direct correlation functions that allow the study of a broad class of crystalline structures. This construction examines planar spacings, lattice symmetries, planar atomic densities and the atomic vibrational amplitude in the unit cell of the lattice and also provides control parameters for temperature and anisotropic surface energies. The power of this new approach is demonstrated by two examples of structural phase transformations.

PACS numbers: 64.70.K-, 61.50.Ah, 81.10.Aj, 46.15.-x

Solid-state transformations form the basis of many problems in materials science and physical metallurgy [1]. They involve complex structural changes between parent and daughter phases and couple atomic-scale elastic and plastic effects with diffusional processes. These phenomena are presently impossible to compute at experimentally relevant time scales using molecular dynamics simulations. On the other hand, meso-scale continuum models wash out most of the relevant atomic scale physics that leads to elasticity, plasticity, defect interactions and grain boundary nucleation and migration. Phase field studies of precipitate and ledge growth [2–4] must thus re-introduce these effects phenomenologically. There is presently no continuum method to efficiently simulate solid-state transformations on diffusional time scales that self-consistently computes elastic and plastic effects at the atomic scale.

Classical density function theory (CDFT) provides a formalism that can accurately describe the emergence of crystalline order from a liquid or solid phase through a coarse-grained density field [5]. Unfortunately, this approach requires very high spatial resolution and is highly inefficient for dynamical calculations [6]. A recent model, coined the phase field crystal (PFC) model, has been gaining widespread recognition as a hybrid method between CDFT and traditional phase field methods. PFC models capture most of the essential physics of CDFT without having to resolve atomically sharp atomic density peaks [7–11]. In spite of their successes, however, only PFC free energy functionals minimized by triangular (2D) or BCC (3D) lattices have been seriously studied. While there have been attempts to extend the PFC model to describe other crystal symmetries such as square [12, 13] and FCC [6, 14, 15] lattices, these have been somewhat ad-hoc and not self-consistently connected to material properties. PFC modeling is presently lacking a generalized free energy formulation that allows the study of important phase transformations between *different* crystalline states.

This Letter proposes a new CDFT/PFC model based on

two-point direct correlation function that is systematically constructed to be minimized by arbitrary crystalline states. The utility and efficiency of our density functional model is demonstrated by dynamically simulating the growth of solid phases into a liquid and the nucleation of precipitate phases within a parent phase of different crystallographic symmetry. We begin with the CDFT free energy functional,

$$\Delta F[n(\vec{r})] = \Delta F_{id}[n(\vec{r})] + \Delta F_{ex}[n(\vec{r})], \quad (1)$$

where ΔF is the free energy difference with respect to a reference state at density ρ_0 [5], and has contributions from a non-interacting term ΔF_{id} and an excess energy ΔF_{ex} . The latter is responsible for the formation of structured phases.

Eq. (1) is expanded around the reference density using the dimensionless number density $n(\vec{r}) = \rho(\vec{r})/\rho_0 - 1$, where $\rho(\vec{r})$ is the local density. The non-interacting contribution is approximated by expanding the Helmholtz free energy of an ideal gas,

$$\begin{aligned} \Delta F_{id} &= \rho_0 k_B T \int d\vec{r} (1 + n(\vec{r})) \ln(1 + n(\vec{r})) - n(\vec{r}) \\ &\approx \rho_0 k_B T \int d\vec{r} \left[\frac{n(\vec{r})^2}{2} - \frac{n(\vec{r})^3}{6} + \frac{n(\vec{r})^4}{12} \right]. \end{aligned} \quad (2)$$

The excess energy is expanded as in CDFT [5] and earlier PFC models [9, 16] up to second order correlations,

$$\Delta F_{ex} = -\frac{\rho_0 k_B T}{2} \int d\vec{r} n(\vec{r}) \int d\vec{r}' (C_2(|\vec{r} - \vec{r}'|) n(\vec{r}')) \quad (3)$$

where $C_2(|\vec{r} - \vec{r}'|)$ is the two particle direct correlation function. The dimensionless number density field $n(\vec{r})$ is evolved in time using conserved dissipative dynamics,

$$\frac{\partial n(\vec{r})}{\partial t} = M \nabla^2 \frac{\delta \Delta F}{\delta n(\vec{r})} + \eta \quad (4)$$

where M is a kinetic mobility parameter and η is conserved random noise. For increased numerical efficiency, Eq. (3) is

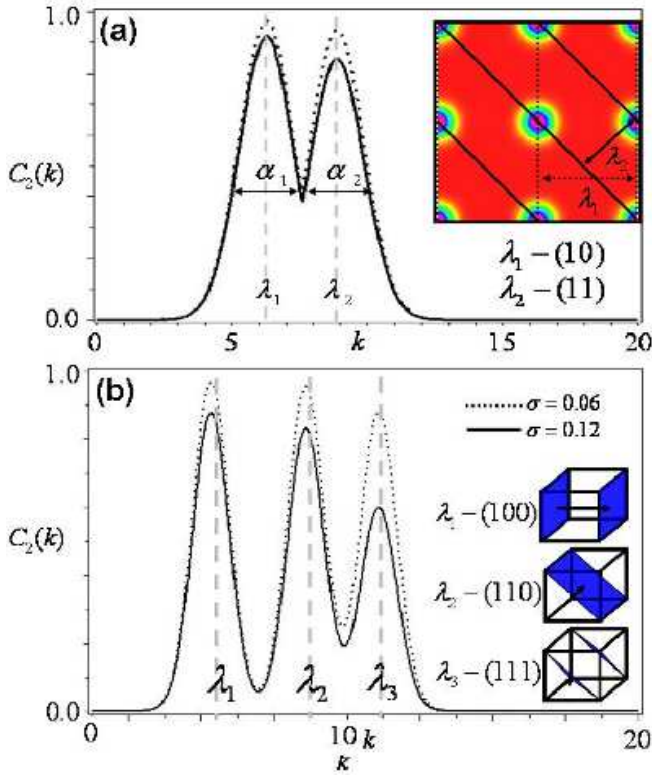


FIG. 1. (a) Direct pair correlation function for a square lattice at two temperatures ($\sigma = 0.82$, solid and $\sigma = 0.5$, dotted, see text). The two peaks in the correlation function each represent one of two planes in the unit cell with interplanar spacings λ_1 and λ_2 (see inset). (b) Correlation function for a simple cubic (SC) lattice at two different temperatures. In 3D, a cubic lattice is represented by three planes in the unit cell. The simple cubic cell has two planar spacings in common with a BCC lattice and requires the third peak to stabilize the structure.

integrated in reciprocal space using a semi-implicit technique [8, 11].

Periodic structures emerge in the phase field crystal model through the input of a direct correlation function into the excess free energy. Here we shall construct correlation functions to create free energy minima for arbitrary crystalline lattices by expanding the free energy functional about a solid state reference density [17]. The original PFC model uses a single mode correlation function; our correlation functions include multiple modes, each of which corresponds to the spacing between atomic planes within a particular unit cell. Figure 1 shows two examples the direct pair correlation function in reciprocal space that generate stable square (a) and simple cubic (SC) (b) lattices when the corresponding free energy is minimized. The functions $C_2(k)$ are constructed in reciprocal space by combining multiple peaks whose position, amplitudes and width are determined as follows:

The number of peaks in the correlation function and their reciprocal space positions are determined by the unit cell of the desired lattice. Every plane within the unit cell produces

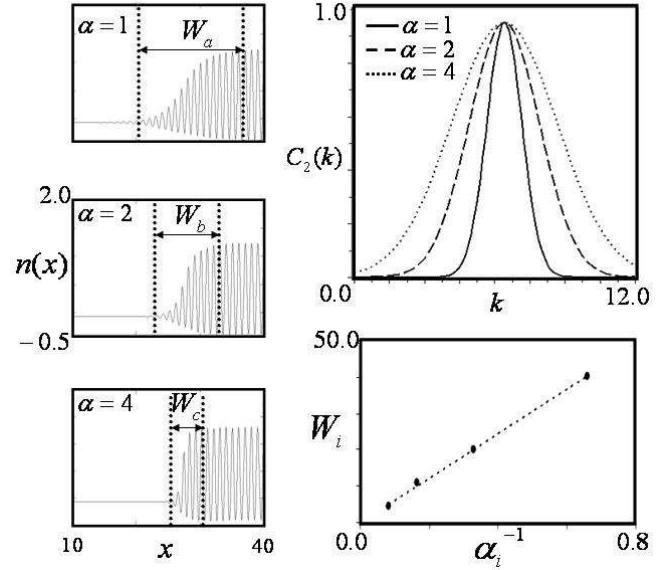


FIG. 2. Effect of peak width α_i in the correlation functions on planar interface width W_i . Left: Three values of α_i and their resulting interface widths. Top Right: Peak shapes corresponding the interface widths to the left. Bottom Right: Dependence of simulated interface width on the fourier space correlation peak width (see text).

a family of peaks derived from the inter-planar spacings. For a 2D square lattice, for instance, the unit cell contains two families of planes, $\{10\}$ and $\{11\}$, with spacings λ_1 and λ_2 as shown in the inset of Figure 1(a). For a perfect crystal, there are an infinite number of peaks located at integer multiples of the wavevector $k_i = 2\pi/\lambda_i$, where i denotes the plane. For square and cubic lattices, it is sufficient to keep only the lowest frequency mode for each family of these peaks in the correlation function for each plane in the unit cell.

Temperature dependence enters the correlation function via modulation of the peak heights through a Debye-Waller factor, denoted P_i . As thermal motion causes atoms to vibrate about their lattice positions, the reciprocal space lattice amplitudes fall off by $e^{-\sigma^2 k_i^2/2}$ where σ is related to the vibrational amplitude of the atoms and thus temperature. The peak height is additionally influenced by the (dimensionless) atomic density ρ_i within a plane and the number of planes β_i in each family. This effect can be seen when integrating out the angular dependence in the reciprocal lattice. Here we modify the Debye-Waller Factor to include both of these effects as $P_i = \exp[-\frac{\sigma^2 k_i^2}{2\rho_i\beta_i}]$. For example, in a square lattice the families of $\{11\}$ and $\{10\}$ planes each consist of 4 sets of planes (ie. the $\{11\}$ family contains (11), $(\bar{1}1)$, $(1\bar{1})$, and $(\bar{1}\bar{1})$) and therefore $\beta_{11} = \beta_{10} = 4$. The (11)-plane has an atomic density $\rho_{11} = 1/\sqrt{2}$ and the (10)-plane has a density of $\rho_{10} = 1$.

The peaks in the reciprocal space correlation function are represented by Gaussians $\exp[-\frac{(k-k_i)^2}{2\alpha_i^2}]$ of finite width α_i rather than the δ -peaks of a perfect lattice. The parameter α_i provides a way to account for changes in the free energy

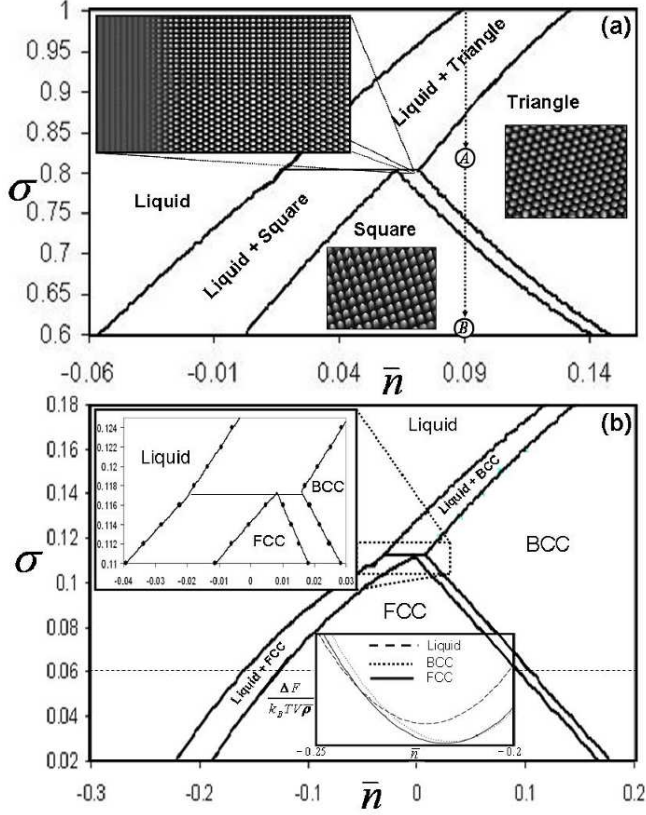


FIG. 3. (a) Phase diagram for a square lattice correlation function showing coexistence between liquid, solid and triangular phases. The inset contains stripes of square and triangular lattices in a liquid phase quenched to a temperature $\sigma = 0.79$. The square phase density was initialized to $n_{sq} = 0.067$ and the triangular phase density to $n_{tri} = 0.076$. The mean density of the system is set to $\bar{n} = 0.07$ and the surface energy parameters are $\alpha_1 = \sqrt{2}$ and $\alpha_2 = 1$. (b) Phase diagram for a FCC correlation function. The insets show the peritectic point and the energy curves for the liquid, FCC and BCC states at temperature of $\sigma = 0.06$.

due to interfaces, defects and strain. The effect of varying α_i on the width of a liquid-solid interface is illustrated in Figure 2. Increasing the value of α_i leads to a decrease in the interface width, which directly affects the surface energy as shown previously by Majaniemi and Provatas [18]. In fact, the relationship between the interface width and the peak width in the correlation function is $1/\alpha_i \propto W_i$ as illustrated in Figure 2. This result can be arrived at by the inverse fourier transform of $C_2(k)$ and agrees well with the traditional phase field models, which incorporate surface energy through square gradients in the order parameter. Note also that α_i incorporates temperature dependence in the surface energy through the Debye-Waller shift of the peak height.

In summary, each family of planes i in the unit cell contributes a peak to the direct pair correlation function of the form

$$C_2(k)_i = e^{-\frac{\sigma^2 k_i^2}{2\rho_i \beta_i}} e^{-\frac{(k-k_i)^2}{2\alpha_i^2}}. \quad (5)$$

The correlation functions seen in Figure 1 are the envelope of the superposition of all relevant peaks for the crystal structure. This construction described above provides a general and robust method by which to generate desired crystal structures, which incorporate temperature dependence through the Debye-Waller factor. This technique also allows for simple control over the surface energy, which can be independently tuned to incorporate anisotropy between planar facets.

By substituting the correlation function into the free energy Eq. (1), the phase diagram is obtained at different temperatures, using the free energy curves obtained for each phase. The energy curves are calculated by an iterative relaxation technique for each structure using the minimal kernel for the structure of interest. For the liquid state, the energy is calculated by imposing a constant density field, and the energy per unit volume is calculated by numerically integrating Eq. (1). For the solid state, the structures corresponding to the correlation function are fit using a Gaussian density field. For example, for the correlation function of Fig. 1(a), density fields for square and triangular lattices with lattice spacings of 1 and $1/\sqrt{3}$ are constructed and relaxed using Eq. (4) to allow the density peaks to obtain an amplitude corresponding to the local minimum energy state. This process is repeated for a series of mean densities to produce energy-density curves for each phase at a given quench. An example of these curves is shown as an inset to Fig. 3(b) for an FCC free energy functional. The double tangent construction is performed for many quenches giving the phase diagrams in Fig. 3(a) for a square correlation function and in Fig. 3(b) for an FCC correlation function.

In both 2D and 3D, we find that the phase that possesses the symmetry of the underlying correlation function emerges at low temperatures and intermediate densities. As the temperature is increased, the lowest frequency mode becomes dominant and for high enough densities, the square (FCC) crystal transforms into a triangular (BCC) crystal. For lower densities, the square (FCC) crystal melts into a homogeneous liquid. Note that our model also predicts a peritectic point in both dimensions, where two solid phases coexist with a liquid. This remarkable feature opens a window into the study of structural phase transformations and structural phase coexistence. Coexistence between FCC crystals with the liquid phase is also easily obtained. Similarly, the correlation function shown in Fig. 1(b) produces coexistence of a liquid and SC phase.

Our new model is applied here to two important examples of nonequilibrium solid state processes. The first is the growth of two structurally different lamellae (stripes) into a liquid phase as illustrated in the inset of Fig. 3(a). The square phase is oriented such that the $\{10\}$ planes are in contact with the liquid phase. Since each peak in the two particle correlation function represents a single plane, the surface energy of the interface is controlled by the width of the corresponding peak. The square phase $\{10\}$ -facet has its surface energy derived from the width α_2 of the second peak of the correlation function, while the triangular phase facets are derived directly from the width α_1 of the first peak. The square phase surface energies can be tuned to isotropy by selecting the proper

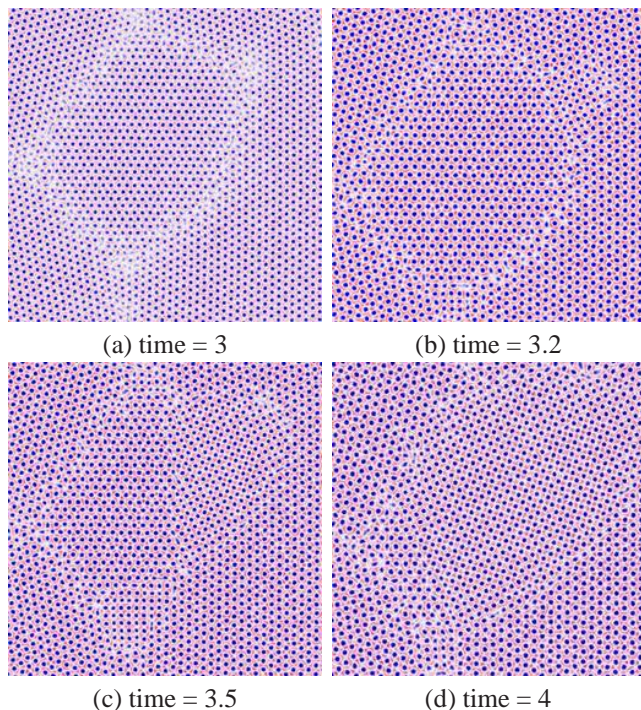


FIG. 4. (Colour Online) 2D nucleation: from triangles to squares. (a) A liquid with density $\bar{n} = 0.09$ is quenched into the triangular region of the phase diagram ($\sigma = 0.82$), marked (A) in Fig. 3(a), produces grains with triangular symmetry. (b-d) A second quench into the square portion of the phase diagram ($\sigma = 0.6$), marked (B) in Fig. 3(a), illustrating the nucleation and subsequent growth of square grains at the vertices of the triangular grains.

ratio of the peak widths. Conversely, anisotropic surface energy can be introduced by increasing or decreasing α_1 while holding α_2 constant. This effect also extends to the solid-solid surfaces between boundaries of different structure (for example, triangle-square boundaries) and misoriented solids of a structure derived from multiple peaks (for example, the square structure). The triangle structure is derived directly from a single peak and is therefore isotropic for a given misorientation. Small changes in the strength of the anisotropy lead to small changes in the angle of the solid liquid interfaces at the vertex point between the three phases.

The second application of interest is the nucleation of a new structural phase by a quench into the second phase region of the phase diagram. For illustrative purposes, the simple 2D case of square-triangle structural transformations is used here. A liquid with a homogenized density field can be quenched into the triangular region of the phase diagram (see point A on the transformation path in Figure 3(a)). Conserved noise in the dynamics is added, and seeds of the triangular phase nucleate and are allowed to coarsen for some time. One such small grain is illustrated in Fig. 4(a). After some time, the material can be further quenched into the square portion of the

phase diagram (see point B). Nucleation of the square phase and subsequent growth and coarsening of the new phase is observed. Note that the nucleation events happen at the vertex positions in the grain structures, as observed in experiments [1]. Two such nucleation points are shown in Fig. 4(b). The orientation of a nucleus and coherency strains can sometimes inhibit the growth of the new phase. This can cause the new phase to be dominated by another nucleation that is in a more favourable position to grow, an effect illustrated in panels (c) and (d) of Fig. 4.

We have introduced new CDFT/PFC free energy functionals for efficient numerical study of solid state transformations. In contrast to earlier work [13], we find that two-point correlations are sufficient to generate stable cubic lattices, and higher order terms in the expansion of ΔF_{ex} can still be neglected. The correlation functions are systematically built up from fundamental principles and desired crystallographic properties of phases of interest at a finite temperature. Our model captures a peritectic transition as well as the nucleation and growth of second-phase precipitates with different crystalline structures.

This work has been supported by the Natural Science and Engineering Research Council of Canada (NSERC).

-
- [1] J. W. Martin, R. D. Doherty, and B. Cantor, *Stability of Microstructure in Metallic Systems second edition* (Cambridge University Press, 1997).
 - [2] D. Yeon, P. Cha, J. Kim, M. Grant, and J. Yoon, *Modelling Simul. Mater. Sci* **13**, 031609 (2005).
 - [3] I. Loginova, A. J. and A. G, *Acta Mat* **52**, 4055 (2004).
 - [4] M. Greenwood, J. Hoyt, and N. Provatas, *Acta Mat* **57**, 2613 (2009).
 - [5] T. Ramakrishnan and M. Yussouff, *Phys Rev B* **19**, 2775 (1979).
 - [6] A. Jaatinen, C. Achim, K. Elder, and T. Ala-Nissila, *Phys. Rev. E* **80**, 031602 (2009).
 - [7] K. Elder, M. Katakowski, M. Haataja, and M. Grant, *Phys Rev Lett* **88**, 245701 (2002).
 - [8] K. Elder and M. Grant, *Phys Rev E* **70**, 051605 (2004).
 - [9] K. Elder, N. Provatas, J. Berry, P. Stefanovic, and M. Grant, *Phys Rev B* **75**, 064107 (2007).
 - [10] P. Stefanovic, M. Haataja, and N. Provatas, *Phys Rev Lett* **96**, 225504 (2006).
 - [11] J. Mellenthin, A. Karma, and M. Plapp, *Phys Rev B* **78**, 184110 (2008).
 - [12] J. Kröger, *Masters Thesis* (McGill University, 2005).
 - [13] P. Tupper and M. Grant, *EPL* **81**, 40007 (2008).
 - [14] K.-A. Wu, *PhD Thesis* (Northeastern University, 2006).
 - [15] G. Tegze, L. Granasy, G. Toth, F. Podmaniczky, A. Jaatinen, T. Ala-Nissila, and T. Pusztai, *Phys. Rev. Lett.* **103**, 035702 (2009).
 - [16] S. Teeffelen, R. Backofen, A. Voigt, and H. Löwen, *Phys Rev E* **79**, 051404 (2009).
 - [17] C. Ebner, H. Krishnamurthy, and R. Pandit, *Phys Rev A* **43**, 4355 (1991).
 - [18] S. Majaniemi and N. Provatas, *Phys Rev E* **79**, 011607 (2009).